# CHAPTER VI
# IMPRESSIVE PHENOL HYDROXYLATION ACTIVITY USING Fe-Ti-TUD-1 SYNTHESIZED FROM SILATRANE VIA SOL-GEL PROCESS

## 6.1 Abstract

Bimetallic Fe–Ti-TUD-1 three-dimensional amorphous mesoporous materials were successfully synthesized via sol–gel method, using tetraethylammonium hydroxide (TEAOH) as a structural directing agent; silatrane, $FeCl_3$, and $Ti(OCH(CH_3)_2)_4$ as silica, iron, and titanium sources, respectively. The obtained Fe–Ti-TUD-1 has a foam-like mesoporous structure with surface area ranging from 625 to 725 $m^2/g$, an average pore size of 6 nm, and a pore volume of 0.97 $cm^2/g$. The phenol hydroxylation of the samples was evacuated using $H_2O_2$ as the oxidant and water as the medium. The effects of influence parameters, such as temperature, reaction time, catalyst amount, amount of oxidant, and metal loading, were investigated; the optimum condition was found to be a ratio of 1:3 phenol:$H_2O_2$, using 30 mg of catalyst at 363 K for 1 h. For comparison, photocatalysis for phenol hydroxylation was studied at room temperature. The result revealed that the activity of 0.01Ti-TUD-1 was improved under UV radiation, but the overall activity resulted in lower performance than the reaction under heat. Phenol hydroxylation using 0.01Fe–0.01Ti-TUD-1 gave 93.1% conversion at 363 K with 53.4% hydroquinone (HQ) and 46.6% catechol (CAT) selectivity. As Fe incorporated into the structure, it improved the catalytic ability of Ti-TUD-1. Unfortunately, the activity of Fe dropped under the UV light since iron species were less active in this condition.

## 6.2 Introduction

Porous materials have been widely used as catalysts, catalyst supports, and adsorbents due to their high surface area available for chemical processes [1]. However, the inability of a bulky substrate to penetrate through the internal pores becomes a problem if the pores are small, as in such materials as zeolites [2]. The reaction of 5-(hydroxymethyl)furfural (HMF) with ethanol using zeolite as a catalyst exhibited fast deactivation due to the pore blocking of organic matter inside the micropore [3]. Fechete *et al* [4] have investigated (Si,Fe)-MCM-22 zeolite in toluene disproportionation. The result showed low percent conversion of toluene since only small p-xylene molecule diffuse faster than the other product, leading to limitation of the reaction. The pore plugging that hinders the diffusion of reactants is also considered as a drawback, especially for those materials having a single-dimensional pore structure, such as MCM-41 [2]. These limitations can be overcome by a new class of three-dimensional amorphous mesostructured silicate TUD-1, having a sponge-like structure with tunable pores, thus providing high substrate accessibility [5]. In $CO_2$ capture of molecular basket sorbents research, Wang *et al* [6] reported that TUD-1 supported polyethylenimine samples performed faster $CO_2$ sorption than SBA-15 and the diffusion constant improved according to 3D structure and large pore size. TUD-1 can be synthesized in an environmentally friendly manner via a low cost, surfactant-free, process, [2]. However, as the siliceous TUD-1 itself lacks catalytic activity, incorporation of heteroatoms, such as Fe [7-8], Co [8], Cu [8-9], Al [10], and Ti [11], into TUD-1 have been investigated. The introduction of multi-components can create new redox and acid properties, as compared with the limitations of mono-heteroatoms. It is of interest if one metal can support the structural and the electronic properties of the other. Therefore, bimetallic catalysts usually improve the catalytic activity, selectivity, and thermal stability of monometallic catalysts. However, only a few studies have reported on the synthesis of bimetallic TUD-1 [12]. One study found that iron-substituted mesoporous materials resulted in a better activity in alkylation and oxidation reactions [13-15], especially in the phenol hydroxylation [16], while titanium containing silicate materials provides not only a good photocatalytic ability [17-18], but also a better

phenol hydroxylation [19]. Due to the same ability of iron- and titanium-substituted mesoporous silicas in the catalytic performance for phenol hydroxylation, in this study, the incorporation of both metal atoms into TUD-1 silicates was synthesized via sol-gel process using homemade silatrane, which has a much better moisture stability than TEOS, as a silica source. The influence parameters, such as temperature, reaction time, catalyst amount, amount of oxidant, and metal loading, were systematically investigated. The product was characterized using XRD, $N_2$ adsorption/desorption, XRF, DRUV-Vis, and TEM. The catalytic activity and stability on phenol hydroxylation were studied.

## 6.3 Experimental

### *6.3.1 Materials*

Fumed silica ($SiO_2$) from Nippon aerosil, iron (III) chloride hexahydrate ($FeCl_3 \cdot 6H_2O$) and tetraethylammonium hydroxide (35%, TEAOH) from Aldrich, titanium (IV) isopropoxide ($Ti(OCH(CH_3)_2)_4$) from Acros Organics, ethylene glycol (EG, $HOCH_2CH_2OH$) from J.T. Baker, triethanolamine (TEA, $(HOCH_2CH_2)_3N$) from QREC, acetronitrile ($CH_3CN$) from Labscan, methanol ($CH_3OH$, 99.9%) (Labscan, Thailand), catechol (CAT, 99%) (Sigma-Aldrich, USA), hydroquinone (HQ, 99%) (Sigma-Aldrich, USA), 1,4-benzoquinone (BQ, 98%) (Sigma-Aldrich, USA), phenol detached crystals (Fisher scientific, UK), hydrogen peroxide ($H_2O_2$, 30% w/v) (Fisher scientific, UK), were used without purification.

### *6.3.2 Synthesis of xFe-yTi-TUD-1*

Synthesis of Fe-Ti-TUD-1 followed the work done by Tunglamlert *et al.* [20] who synthesized Ti-TUD-1. The molar ratio composition was $SiO_2$:0.7TEAOH:$14H_2O$:*x*Fe:*y*Ti, where $0.01 \leq x,y \leq 0.09$ was prepared by adding a required amount of $FeCl_3 \cdot 6H_2O$ in 0.90 g of water, followed by dissolving 4.50 g of silatrane and stirring for 1 h. 4.21 g of TEAOH was added dropwise into the mixture, followed by adding a desired amount of $Ti(OCH(CH_3)_2)_4$. After aging for 2 h at room

temperature, the synthesized solution was dried at 373 K for 24 h. The organic residue was removed by calcination at 873 K for 10 h using a heating rate of 1°C/min. TUD-1, Fe-TUD-1 and Ti-TUD-1 were also synthesized using the same procedure for comparison.

### *6.3.3 Characterization*

XRD patterns were recorded using CuKα radiation on a Rigaku diffractometer. Nitrogen physisorption isotherms were measured on a Quantasorb JR instrument using the Brunauer-Emmett-Teller (BET) method. Diffuse reflectance UV-vis (DRUV) spectra were performed using a Shimadzu UV-2550. XRF was carried out on a PANalytical AXIOS PW 4400. TEM micrographs were obtained using a JEOL JEM-2010. High performance chromatography (HPLC, SPD-M20A Shimadzu) equipped with a C-18 reverse-phase column (Inertsil ODS-3) using 10 vol% acetronitrile and 10 vol% methanol in water as a mobile phase at a flow rate of 1.0 ml/min and a UV detector operating at 254 nm was used to analyze the activity study products.

### *6.3.4 Catalytic Activity Study*

Phenol hydroxylation was carried out in two systems: thermal and photocatalytic systems. In the thermal reaction, a 50 ml reaction flask fitted with a water condenser was heated at 303–363 K. Phenol (1.88 g, 20 mmol) and 30% aqueous $H_2O_2$ (2.28 g, 20 mmol) were mixed in 10 ml of water before heating the mixture in an oil bath with vigorous stirring [21]. For the photocatalytic study, the same solution as the hydrothermal study before heating was exposed to UV light from a UV lamp (100 W Hg Sylvania UV lamp). The reaction products were analyzed by HPLC. All reactions were repeated three times and average values were used in the data presentation.

### *6.3.5 Leaching and recycling of the catalysts*

Leaching of metal ions from the catalyst was investigated at 363 K. The catalyst sample was filtered off after 30 min reaction time and allowed the reaction mixture to undergo further reaction in the oil bath at the same temperature for 1 h. The solutions before and after filtration were analyzed by HPLC. The filtered catalyst was washed with distilled water, dried, and calcined at 773 K for 2 h before carrying out the next run.

### *6.3.6 Hydrothermal stability test*

After running the reaction at 363 K for 1 h, the catalysts were recovered by filtration, washed with distilled water, and calcined at 773 K for 2 h. The stability of the samples was analyzed using XRD and nitrogen adsorption.

## 6.4 Results and Discussion

### *6.4.1 Characterization of Catalyst*

The XRD patterns of calcined metallic TUD-1 and M-TUD-1 (Fig. 6.1a and b) show an intense peak at 0.6° 2θ which confirms an amorphous mesostructured material of TUD-1 [9-11]. Ti-TUD-1 samples with a Ti/Si ratio between 0.01 and 0.09 (Fig. 6.1a) were successfully synthesized using titanium(IV) isopropoxide as a titanium source because the hydrophobic force between isopropoxide and TEAOH can stabilize the structure of TUD-1[10]. Fe-TUD-1 with an Fe/Si ratio over 0.03 cannot be achieved with the foam-like mesostructure formation due to the less effective anionic chloride ion of the iron precursor, causing an imbalance of charge matching at high concentration [22]. It may be seen in Fig. 6.1a that the intensities of both Fe- and Ti-TUD-1 peaks decreased, diffraction peaks slightly shift to higher 2θ value and d-spacing decreased as the metal amount increased because more iron and titanium atoms, whose sizes are larger than silicon atom, were cooperating in TUD-1 and causing the TUD-1 structure to be distorted.

Bimetallic samples of xFe-yTi-TUD-1with $0.01 \leq x \leq 0.03$ and $0.01 \leq y \leq 0.09$ provided a 3D sponge-like mesostructure of TUD-1 with the absence of the peak characteristics of $TiO_2$ and $Fe_2O_3$ nanoparticles, as observed by wide angle XRD patterns (not shown).

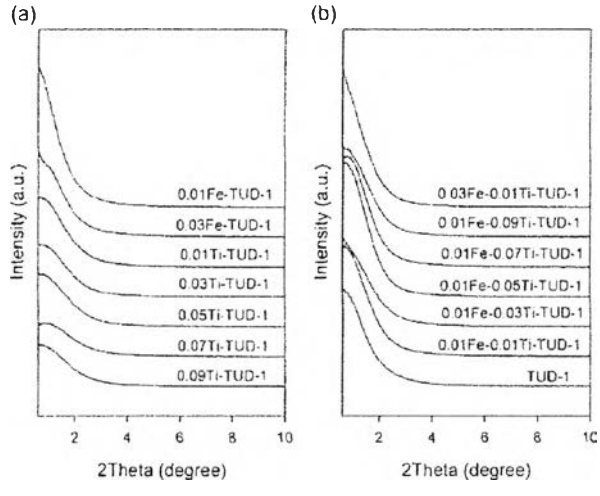


**Figure 6.1** XRD patterns of a) Fe-TUD-1, Ti-TUD-1, b) Fe-Ti-TUD-1, TUD-1.

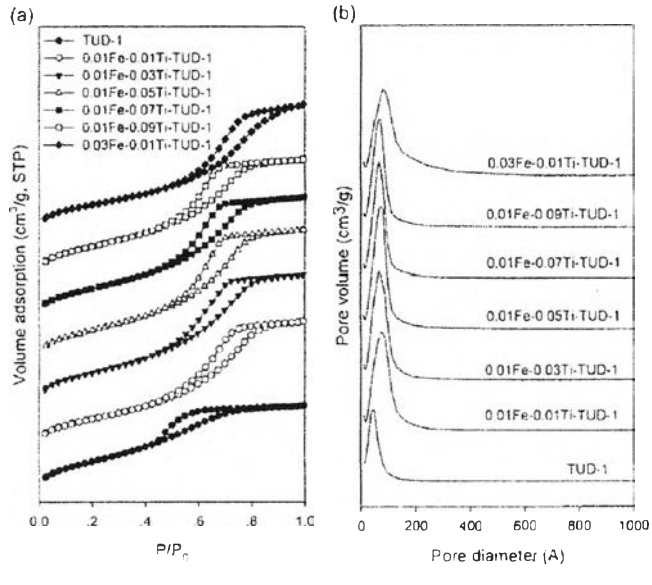


**Figure 6.2** a) $N_2$ adsorption/desorption isotherms, b) pore size distributions of TUD-1, Fe-Ti-TUD-1.

**Table 6.1** Textural properties of TUD-1 and metal modified TUD-1

| Sample | Fe/Si* (mole ratio) | | Ti/Si* (mole ratio) | | BET surface area | pore volume | pore diameter |
|---|---|---|---|---|---|---|---|
| | Gel | Product | Gel | Product | ($m^2/g$) | ($cm^2/g$) | (nm) |
| TUD-1 | 0 | 0 | 0 | 0 | 691 | 0.69 | 4.01 |
| 0.01Fe-TUD-1 | 0.01 | 0.006 | 0 | 0 | 595 | 0.85 | 5.75 |
| 0.03Fe-TUD-1 | 0.03 | 0.015 | 0 | 0 | 572 | 0.95 | 6.63 |
| 0.01Ti-TUD-1 | 0.01 | 0 | 0.01 | 0.006 | 774 | 0.80 | 4.12 |
| 0.03Ti-TUD-1 | 0.03 | 0 | 0.03 | 0.021 | 825 | 0.87 | 4.22 |
| 0.05Ti-TUD-1 | 0.05 | 0 | 0.05 | 0.038 | 777 | 0.95 | 4.90 |
| 0.07Ti-TUD-1 | 0.07 | 0 | 0.07 | 0.051 | 810 | 0.81 | 4.00 |
| 0.09Ti-TUD-1 | 0.09 | 0 | 0.09 | 0.069 | 752 | 0.74 | 3.95 |
| 0.01Fe-0.01Ti-TUD-1 | 0.01 | 0.006 | 0.01 | 0.006 | 672 | 0.98 | 5.84 |
| 0.01Fe-0.03Ti- TUD-1 | 0.01 | 0.006 | 0.03 | 0.019 | 725 | 1.01 | 5.56 |
| 0.01Fe-0.05Ti- TUD-1 | 0.01 | 0.007 | 0.05 | 0.033 | 707 | 1.02 | 5.76 |
| 0.01Fe-0.07Ti-TUD-1 | 0.01 | 0.006 | 0.07 | 0.048 | 685 | 0.94 | 5.52 |
| 0.01Fe-0.09Ti-TUD-1 | 0.01 | 0.008 | 0.09 | 0.058 | 664 | 0.90 | 5.45 |
| 0.03Fe-0.01Ti-TUD-1 | 0.03 | 0.019 | 0.01 | 0.007 | 625 | 0.99 | 6.32 |

* Data were obtained from XRF.

Figures 6.2a and 6.2b show the $N_2$ adsorption isotherms and pore size distribution of TUD-1 and Fe-Ti-TUD-1 containing different metal contents. Bimetallic Fe-Ti-TUD-1 and TUD-1 samples exhibit narrow pore size distribution (Fig. 6.2b) with type IV IUPAC adsorption isotherm, which is a characteristic of mesoporous material. The hysteresis loops of type $H_2$ are observed and indicate the pore blocking/percolation effects of disordered materials [23]. Fe-Ti-TUD-1 samples generated steeper hysteresis loops (see Fig. 6.2a) than siliceous TUD-1 since the formation of nano-particles of metal oxide inside the pores smoothed the inner surface of TUD-1, as discussed by Hamdy [24]. Textural properties of TUD-1 and metal-modified TUD-1 are summarized in Table 6.1. BET surface areas of all samples were obtained in a range of 572–825 $m^2/g$ with a pore volume range of 0.69–1.02 $cm^2/g$. Interestingly, Ti-TUD-1 and Fe-Ti-TUD-1 show smaller particle size than the pure TUD-1 (not shown). causing the surface areas to be higher. However, for all mono-and bimetallic TUD-1, the pore volumes were larger than the pure TUD-1. This is due to the presence of the large iron (Paulling radius = 64 pm) and titanium atoms (Paulling radius = 60 pm), compared with silicon atom (Paulling radius = 42 pm), in the framework, as explained by Ramanathan et al. [25]. All samples showed a pore diameter around 4–7 nm. As the titanium amount was increased in Fe–Ti-TUD-1, there was no effect on the pore size distribution, while the introduction of high iron content caused a broad peak of pore size distribution which shifted in the larger pore size than TUD-1. This might be due to the partial deposition of small Fe cluster inside the pore, extending the pore diameter [26].

The total amounts of metals in Fe-TUD-1, Ti-TUD-1 and Fe-Ti-TUD-1 were also determined using XRF spectroscopy, as summarized in Table 6.1. It is revealed that the actual contents of Fe and Ti introduced into the framework of TUD-1 were less than the composite gels, probably due to the solubility of Fe and Ti precursor in the basic medium.

The incorporation of Ti and Fe into the TUD-1 framework was verified by DRUV-Vis spectroscopy. The UV-Vis spectra of all calcined samples are shown in Fig. 6.3. The adsorption band is absent for TUD-1, while Fe-TUD-1 samples with Fe/Si ratios of 0.01 and 0.03 shown in Fig. 6.3a performed the intense adsorption band between 200 and 230 nm, attributed to the charge-transfer

transitions involving isolated $Fe^{3+}$in $Fe^{3+}O_4$ tetrahedral coordination [27-28]. The adsorption band between 300 and 400 nm observed for the Fe-TUD-1 consisted of some Fe-O-Fe clusters with isolated Fe sites of Si-O-Fe bonds [28]. In addition, $Fe^{3+}O_6$ octahedral coordination at 400-600 nm was also present in the Fe-TUD-1 samples, indicating that these samples had the ferric oxide species as the extraframework [28]. Ti-TUD-1 samples with Ti/Si ratios of 0.01 to 0.09 seen in Fig. 6.3a showed a strong UV band at 200 nm, the characteristic of $Ti^{4+}O_4$tetrahedral titanium sites [20]. A broad band between 240 and 300 nm of Ti-TUD-1 with Ti/Si over 0.01 indicated the oligomeric Ti-O-Ti species [20]. However, the octahedral anatase phase at 330 nm was not detected. The addition of both Fe and Ti resulting in the Fe-Ti-TUD-1 samples (Fig. 6.3b) provides both the tetrahedral coordinations of isolated $Fe^{3+}$ and $Ti^{4+}$ at 200 nm. Some Ti-O-Ti species at 250–300 nm, small Fe-O-Fe clusters at 300–400 nm, and octahedral ferric oxide extraframework at 400–600 nm were also observed. However, a small amount with small size of titanium and iron oxide caused the characteristics of metal oxides to elude wide angle XRD (not shown) and TEM results.

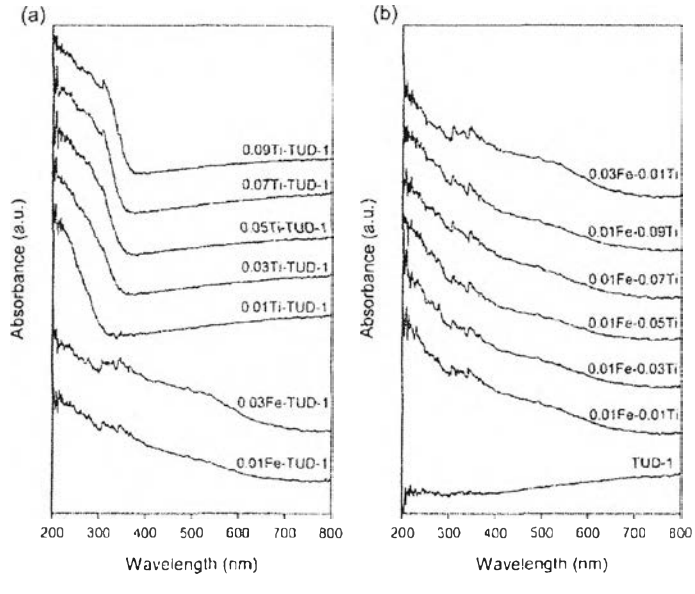


**Figure 6.3** DR UV-vis spectra of (a) Fe-TUD-1, Ti-TUD-1, (b) Fe-Ti-TUD-1, TUD-1.

Table 6.2 exhibits the band gap energies of Fe-TUD-1 and Ti-TUD-1, calculated from UV-vis spectra (See appendices for calculation). The band gap energy of bimetallic Fe-Ti-TUD-1 could not be obtained because $Fe^{3+}$ and $Ti^{4+}$ peaks were overlapped. As the amount of Fe increased, the band gap decreased from 2.609 to 2.472 eV. The red shift of UV-vis spectra occurred at the higher Fe and Ti concentrations; the corresponding band gaps narrowed from 2.609 to 2.472 eV for Fe-TUD-1 and 2.418 to 2.036 eV for Ti-TUD-1. The band gap decreased with increasing the dopant concentration, as also reported by Serpone [46] and Oleksek *et al.*[47]. Therefore, the electron in the valence band would be easily excited to the conduction band due to a narrower band gap [48].

**Table 6.2** Band gap energy of metal modified TUD-1

| Materials | Wavelength (nm) | Band gap energy (eV) |
|---|---|---|
| 0.01Fe-TUD-1 | 601.3 | 2.609 |
| 0.03Fe-TUD-1 | 608.8 | 2.472 |
| 0.01Ti-TUD-1 | 475.0 | 2.418 |
| 0.03Ti-TUD-1 | 501.3 | 2.401 |
| 0.05Ti-TUD-1 | 512.6 | 2.208 |
| 0.07Ti-TUD-1 | 516.3 | 2.061 |
| 0.09Ti-TUD-1 | 561.3 | 2.036 |

TEM images of TUD-1, 0.01Fe-TUD-1, 0.01Ti-TUD-1 and 0.01Fe-0.03Ti-TUD-1 are given in Fig. 6.4a-d, respectively. All samples exhibited a sponge-like 3D mesoporous structure [9,29]. The small size of metal oxides was not seen in the TEM images probably due to the presence of too small an amount of metal oxide particles to fulfill the rough disordered surface without blocking the pore, as resulted in the $N_2$ adsorption isotherms. The dark domain in TEM image is the thick area of the particle which might occur from the analysis preparation process. This dark area didn't show any phase of the nanoparticle as reported by Zhou et al. [29]. This is possibly the result of small nanocluster highly dispersion in the structure.

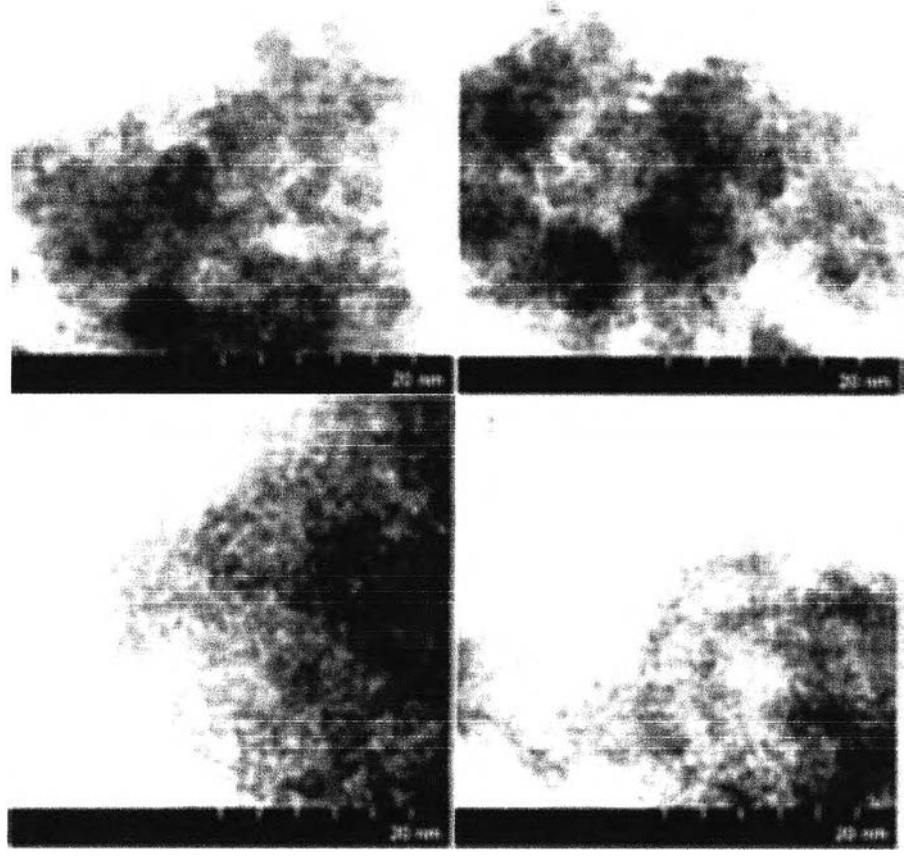

**Figure 6.4** TEM images of a) TUD-1, b) 0.01Fe-TUD-1, c) 0.01Ti-TUD-1, and d) 0.01Fe0.03Ti-TUD-1.

### *6.4.2 Catalytic activity of Fe-Ti-TUD-1*

#### *6.4.2.1 Effects of reaction temperature and reaction time*

Catalytic activity of Fe-Ti-TUD-1 with 0.01Fe/Si and 0.03Ti/Si ratio for phenol hydroxylation at different temperatures is given in Fig. 6.5. As increasing the temperature from 303 K (ambient temperature) to 363 K, the phenol conversion was enhanced up to 61.0%. At early stage of the conversion, the high amount of BQ was produced, as obviously seen at 303 K, due to the over-oxidation of HQ with the excess $H_2O_2$ [31-32]. However, the BQ selectivity

decreased as the conversion increased. In addition, Klaewkla et al. [32] reported that the formation of BQ was highly dependent on the concentration of $H_2O_2$ and independent with reaction time. With the reaction time prolonged or the temperature increased, the thermodynamic product, HQ, was formed, as can be seen at the third hour of the ambient temperature and the initial time of the thermal condition (323–363 K) [33]. CAT was observed at every temperature since the kinetic lower energy pathway was achieved [33]. Therefore, the optimal time and temperature to obtain 61.0% conversion was at 363 K for 30 min.

*6.4.2.2 Effect of the catalyst content*

Figure 6.6 shows the performance of 0.01Fe-0.03Ti-TUD-1 at various catalyst contents, ranging from 10 to 70 mg. The conversion increased from 17.9 to 53.8 % as the catalyst content increased from 10 to 30 mg due to the presence of more active sites [34]. The results from increasing the content to 50 and 70 mg indicated a drop of % conversion to around 50, suggesting that a larger catalyst content, providing more surface area for $H_2O_2$ to associate, formed the active intermediate too fast to affect the oxidative reaction [21]. All catalyst contents studied resulted in a high HQ selectivity. It can be concluded that the thermodynamic product was more favorable as introduced heat [33] and there was no relevant between the product selectivity and the catalyst content. Optimal catalyst content for the phenol hydroxylation was 30 mg with 53.2% HQ and 46.8% CAT selectivity.

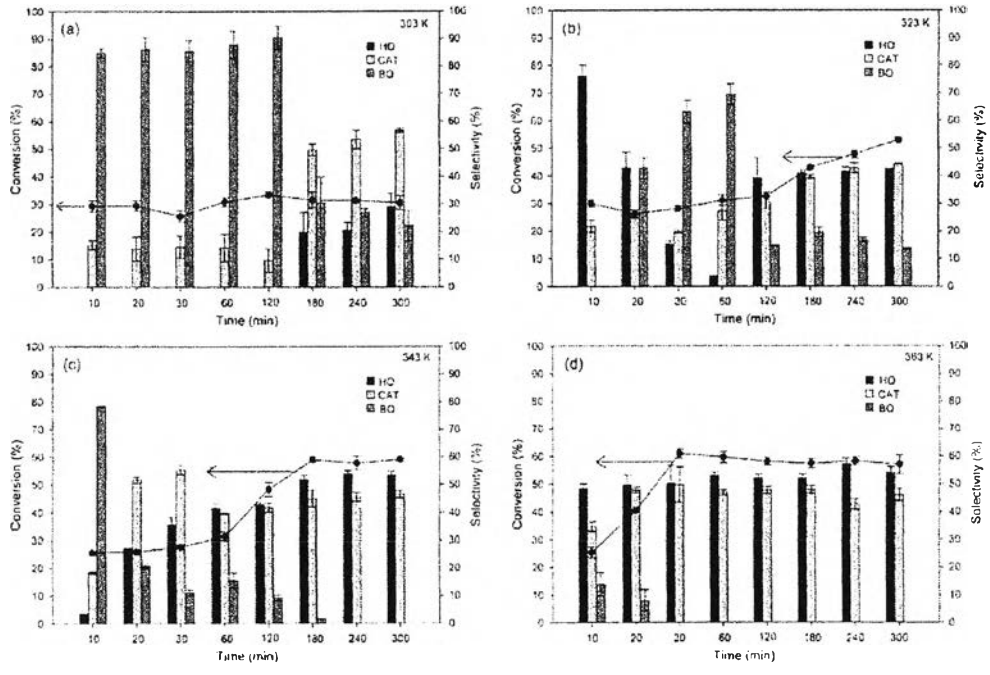


**Figure 6.5** The phenol conversion and the product selectivity of 0.01Fe0.03Ti-TUD-1 (30 mg) using 1:1 phenol:$H_2O_2$ at a) 303, b) 323, c) 343, and d) 363 K for 5 h reaction time.

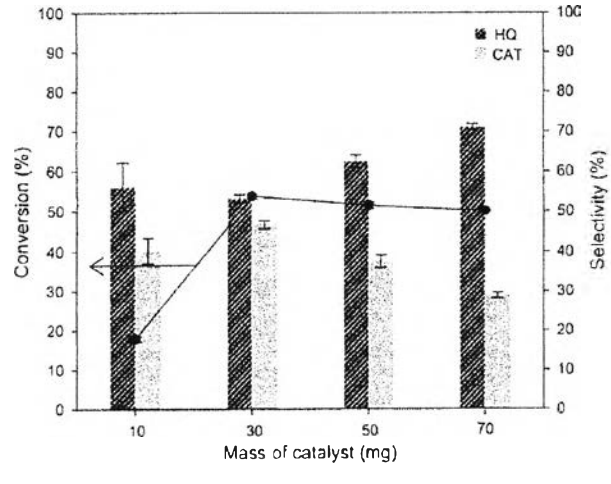


**Figure 6.6** The phenol conversion and the product selectivity of 0.01Fe0.03Ti-TUD-1with respect to the used catalyst amount using 1:1 phenol: $H_2O_2$ at 363 K for 1 h reaction time.

*6.4.2.3 Effect of phenol:$H_2O_2$ molar ratio*

The influence of phenol:$H_2O_2$ molar ratio was investigated and the results are shown in Fig. 6.7. With the increase of $H_2O_2$ amount, the phenol conversion was dramatically increased. At the low molar ratio of 2:1, the phenol conversion reached 38.0%. As decreasing the phenol:$H_2O_2$ molar ratio (or increasing the $H_2O_2$ content) from 1:1 to 1:3, the conversion increased from 53.8 to 90.5% due to more hydroxyl radical reactive species generated from the decomposition of $H_2O_2$ [35-36]. However, the oxidant concentration did not seem to have any effect on the product selectivity which showed a higher HQ selectivity than CAT. Thus, the 1:3 phenol:$H_2O_2$ molar ratio giving the maximum 90.5% conversion was selected as the optimum condition.

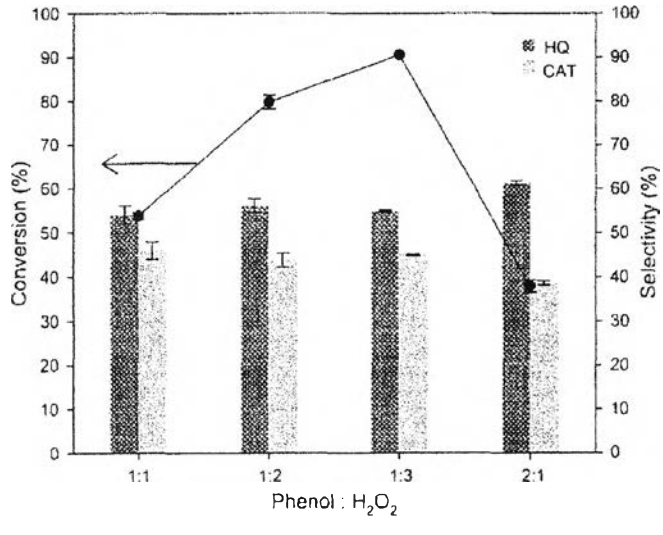


**Figure 6.7** The phenol conversion and the product selectivity of 0.01Fe0.03Ti-TUD-1(30 mg) using various phenol:$H_2O_2$ molar ratios at 363 K for 1 h reaction time.

**Table 6.3** Effect of metal loading onto TUD-1 for phenol hydroxylation using $H_2O_2$ under thermal condition

| Catalyst | Conversion (%) | Selectivity (%) | | | CAT/HQ |
|---|---|---|---|---|---|
| | | HQ | CAT | BQ | |
| No catalyst | 2.2 | 0 | 7.7 | 92.3 | - |
| TUD-1 | 3.5 | 0 | 16.9 | 83.1 | - |
| 0.01Fe-TUD-1 | 93.2 | 55.8 | 44.2 | 0 | 0.79 |
| 0.03Fe-TUD-1 | 26.5 | 35.4 | 54.8 | 9.8 | 1.55 |
| 0.01Ti-TUD-1 | 8.3 | 22.3 | 36.2 | 41.6 | 1.62 |
| 0.03Ti-TUD-1 | 10.1 | 26.7 | 35.1 | 38.3 | 1.31 |
| 0.05Ti-TUD-1 | 10.6 | 15.7 | 10.8 | 73.5 | 0.69 |
| 0.07Ti-TUD-1 | 11.2 | 15.8 | 6.9 | 77.3 | 0.44 |
| 0.09Ti-TUD-1 | 13.6 | 0.7 | 0.8 | 98.5 | 1.14 |
| 0.01Fe-0.01Ti-TUD-1 | 93.1 | 53.4 | 46.6 | 0 | 0.87 |
| 0.01Fe-0.03Ti- TUD-1 | 90.5 | 55.0 | 45.0 | 0 | 0.82 |
| 0.01Fe-0.05Ti- TUD-1 | 40.5 | 35.1 | 60.9 | 4.1 | 1.74 |
| 0.01Fe-0.07Ti-TUD-1 | 25.2 | 34.8 | 52.4 | 12.8 | 1.51 |
| 0.01Fe-0.09Ti-TUD-1 | 14.6 | 24.2 | 46.8 | 29.0 | 1.93 |
| 0.03Fe-0.01Ti-TUD-1 | 28.2 | 30.0 | 57.7 | 12.3 | 1.92 |

Reaction conditions: Phenol: $H_2O_2$ = 1:3, catalyst = 30 mg, T = 363 K, reaction time = 1 h.

**Table 6.4** Effect of metal loading onto TUD-1 for phenol hydroxylation using $H_2O_2$ under UV light

| Catalyst | Conversion (%) | Selectivity (%) | | |
|---|---|---|---|---|
| | | HQ | CAT | BQ |
| No catalyst | 2.23 | 0 | 0 | 100 |
| TUD-1 | 11.1 | 0 | 9.8 | 90.2 |
| 0.01Fe-TUD-1 | 14.3 | 0 | 14.8 | 85.2 |
| 0.03Fe-TUD-1 | 14.8 | 0 | 0 | 100.0 |
| 0.01Ti-TUD-1 | 10.7 | 0 | 23.4 | 76.6 |
| 0.03Ti-TUD-1 | 14.9 | 0 | 11.3 | 88.8 |
| 0.05Ti-TUD-1 | 19.3 | 0 | 2.5 | 97.6 |
| 0.07Ti-TUD-1 | 19.8 | 0 | 1.0 | 99.0 |
| 0.09Ti-TUD-1 | 5.7 | 0 | 0 | 100.0 |
| 0.01Fe-0.01Ti-TUD-1 | 17.4 | 0 | 11.0 | 89.0 |
| 0.01Fe-0.03Ti- TUD-1 | 19.1 | 0 | 8.3 | 91.7 |
| 0.01Fe-0.05Ti- TUD-1 | 14.7 | 0 | 3.3 | 96.7 |
| 0.01Fe-0.07Ti-TUD-1 | 17.1 | 0 | 1.7 | 98.3 |
| 0.01Fe-0.09Ti-TUD-1 | 7.1 | 0 | 2.3 | 97.7 |
| 0.03Fe-0.01Ti-TUD-1 | 14.5 | 0 | 0 | 100.0 |

Reaction conditions: Phenol: $H_2O_2$ = 1:3, catalyst = 30 mg, T = room temperature, reaction time = 1 h.

*6.4.2.4 Effect of metal loading*

Under optimum conditions obtained from above, series of TUD-1, Fe-TUD-1, Ti-TUD-1, and Fe-Ti-TUD-1 were utilized for the phenol hydroxylation, as resulted in Tables 6.2 and 6.3. From Table 6.2, pure TUD-1 and no catalyst systems had very low conversions (only 2.2 and 3.5%, respectively), clearly proving that TUD-1 lacked of active site. Hence the ability to generate the hydroxyl radical was similar to the system containing no catalyst [36]. On the other hand, the 0.01Fe-0.03Ti-TUD-1 system without $H_2O_2$ gave no conversion either (not shown) due to no hydroxyl radical to react with the catalyst. As introduced the metal to TUD-1, the catalytic ability was improved as a result of oxygen transfer properties [36]. The maximum 93.2% phenol conversion was achieved when using 0.01Fe-TUD-1 catalyst. However, further increase of the iron content to 0.03 Fe/Si molar ratio led to a decrease in the catalytic activity, 26.5% conversion, due to the formation of $Fe_2O_3$ on the surface of catalyst, as indicated in the DRUV result [37]. Although, in the case of Ti-TUD-1, the conversion increased with the increase of the titanium content from 0.01 to 0.09 Ti/Si molar ratio, titanium loaded TUD-1 provided much lower performance than iron loaded TUD-1.

For bimetallic Fe-Ti-TUD-1 with 0.01 Fe/Si ratio and 0.01–0.09 Ti/Si ratio, the percentage of conversion decreased from 93.1 to 14.6 as the Ti content increased. Both 0.01Fe-0.01Ti-TUD-1 and 0.01Fe-0.03Ti-TUD-1 had high conversions which were 93.1 and 90.5%, respectively. The selectivity of HQ was higher than CAT and CAT/HQ ratio was less than 1 because most reaction occurred at internal surface which caused geometric strains from the coordination of water to the active site [38]. Thus, HQ was more favorable product inside the pore, consistent to the report of Wróblewska [38]. When Ti amount increased from 0.05 to 0.09 Ti/Si molar ratio, the catalytic ability decreased from 40.5 to 14.6% conversion. The product became more selective with CAT than HQ, and CAT/HQ ratio was over than 1. Since the extraframework metal oxide was formed at high metal loading, the high conversion thus occurred at the external surface; the geometric strains were low enough for CAT to form favorably [38]. It is worth noting that when the phenol conversion was low, resulting in large oxidant amount left, over-oxidation occurred and provided BQ [31-32], as can be seen in the case of a high metal content (0.03Fe-TUD-1, (0.01-0.09) Ti-TUD-1, 0.01Fe-(0.05-0.09) Ti-TUD-1 and 0.03Fe-0.01Ti-

TUD-1). In addition, BQ was also found in the pure TUD-1 and no catalyst systems. As the Fe content increased to 0.03 Fe/Si molar ratio for bimetallic TUD-1, the percentage of conversion decreased to 28.2. This is due to the occurrence of the extraframework $Fe_2O_3$, as discussed earlier, resulting in a lower catalytic ability [37-38]. Comparing between Ti-TUD-1 and Fe-Ti-TUD-1, bimetallic TUD-1 significantly improved the catalytic ability, however, when comparing thermal and UV light treatments, 0.01Fe-TUD-1 provided a much better activity in the thermal condition because the active Fe species in the system causes more production of hydroxyl radicals [38].

The results from the UV light treatment at room temperature on the phenol hydroxylation were summarized in Table 6.3. Expectedly, for a system without $H_2O_2$ (not shown), the reaction did not occur because of no hydroxyl reactive radical generator. Similar to the thermal treatment, the system containing pure TUD-1 or no catalyst, a low phenol conversion was observed (2.23 and 11.1%, respectively) owing to no metal center to enhance the redox properties [35]. In the no catalyst system, only BQ was produced due to the excess amount of $H_2O_2$ causing an over-oxidation reaction [30] and [31]. An increase of the iron content gave no effect on the phenol conversion while the titanium content from 0.01 to 0.07 Ti/Si molar ratio slightly increased the phenol conversion from 10.7 to 19.8%. The conversion dropped to 5.7% as the titanium content increased to 0.09 Ti/Si molar ratio. The high titanium content caused a decrease in the light penetration by the suspended particle, resulting in the activity drop [39]. Unlike the thermal condition, Fe–Ti-TUD-1 gave a low percentage of phenol conversion from 14.7 to 19.1 as the titanium content increased from 0.01 to 0.07 Ti/Si molar ratio, and decreased to 7.1% when the titanium increased to 0.09 Ti/Si molar ratio. This is also owing to the shielding effect of the suspended particle [39]. Undoubtedly, titanium improved the photocatalytic ability of TUD-1 better than iron as the metal content increased. The conversion showed very little change for iron incorporated TUD-1 because titanium gave a much better interaction enhancement between phenol and hydroxyl radicals than Fe [39]. The other possibility is $Fe^{3+}$ narrows the band gap above the valence band of titanium that was present in the structure, enhancing the electron/hole recombination properties that results in 0.01Fe–0.01Ti-TUD-1 and 0.01Fe–0.03Ti-TUD-1 thus

improving the activity of Ti-TUD-1 at the same Ti content [40]. However, the ability of Fe–Ti-TUD-1 dropped at the high Ti content because of the shielding effect as previously discussed. The activity of 0.01Fe–0.01Ti-TUD-1 and 0.01Fe–0.03Ti-TUD-1 was also lower than thermal condition owing to limiting of oxidizing power [40]. As a conclusion, under UV irradiation, titanium incorporated TUD-1, including bimetallic TUD-1, was more effective. BQ was the favorable product for all catalysts and HQ was not detected under UV light exposure. BQ with 100% conversion was achieved for 0.03Fe-TUD-1, 0.09Ti-TUD-1, and 0.03Fe–0.01Ti-TUD-1. A possible reason for not producing HQ was from the strength of the UV light used (100 W) which was insufficient energy inconvert BQ to HQ, a higher energy molecule [41]. Some CAT product was observed for most catalysts since it is the kinetically favorable product [32].

*6.4.2.5 Leaching and reusability of catalysts*

The 0.01Fe–0.01Ti-TUD-1 catalyst was filtered off after 30 min reaction time and the liquid part was allowed to undergo further reaction for investigation of the phenol conversion. It was found that at 30, 40, 50, and 60 min reaction time the phenol conversions were 31.4, 36.3, 60.3, and 72.1, respectively. A gradual increase was implied that iron ion was leached out from the catalyst solid, probably due to the extraframework iron oxide leached easily [42] and [43]. Moreover, the reaction condition under the strong oxidant ($H_2O_2$) leads to leaching of active sites via solvolysis of weak M-O-Si bonds [44]. This result is consistent with the results obtained from the study of the catalyst reusability (not shown) indicating that, after three runs, the phenol conversion was dramatically decreased from 93.4% at the first run to 24.9 and 22.2% at the second and the third runs, respectively.

*6.4.2.6 Hydrothermal stability*

Figure 6.8 presents the $N_2$ adsorption isotherms and pore size distributions of 0.01Ti-TUD-1, 0.01Fe-TUD-1, and 0.01Fe-0.01Ti-TUD-1 after testing the hydrothermal stability at 363 K for 1 h. All samples indicated Type IV isotherms, corresponding to mesoporous material. Specific surface areas of 0.01Ti-TUD-1, 0.01Fe-TUD-1, and 0.01Fe-0.01Ti-TUD-1 were 657, 674, and 617 $m^2/g$ with pore sizes of 5.54, 4.96, and 5.45 nm, respectively. Comparing to Fig. 6.2 showing the catalysts before the hydrothermal treatment, the pore size distributions

of the samples after the hydrothermal treatment were broader due to some structural destruction and some leaching out of the metal during the thermal reaction [30].

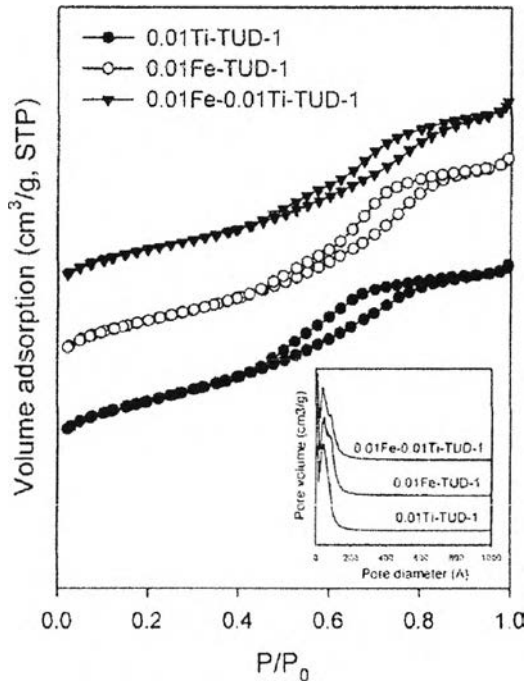


**Figure 6.8** $N_2$ adsorption/desorption isotherms and pore size distributions of 0.01Ti-TUD-1, 0.01Fe-TUD-1, and 0.01Fe-0.01Ti-TUD-1 after hydrothermal stability test at 363 K for 1 h.

Figure 6.9 illustrates the XRD patterns of 0.01Fe-TUD-1, 0.01Ti-TUD-1 and 0.01Fe-0.01Ti-TUD-1 after hydrothermal stability test at 363 K for 1 h. The characteristic peak of the samples around 1.5° still remained. However, the intensity of bimetallic TUD-1 was low probably due to the different sizes of Fe and Ti that distorted the structure, resulting in some collapse of TUD-1.

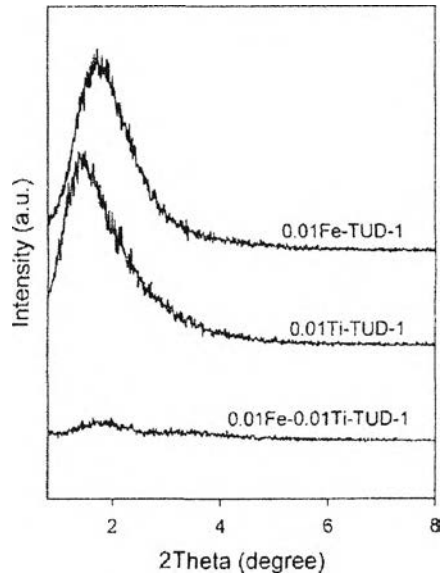


**Figure 6.9** XRD patterns of 0.01Fe-TUD-1, 0.01Ti-TUD-1, and 0.01Fe-0.01Ti-TUD-1 after hydrothermal stability test at 363 K for 1 h.

## 6.5 Conclusions

Fe–Ti-TUD-1 mesoporous materials were successfully synthesized using silatrane as a silica source via sol–gel process. TUD-1 with high iron content could not be prepared while the incorporation of titanium retained the mesopore structure even at high titanium amount. Small titanium and iron oxide clusters were observed and all samples exhibited high surface areas with narrow pore size distribution. The optimum reaction condition was 1:3 of phenol:$H_2O_2$ ratio using 30 mg of catalyst at 363 K. 1 h for thermal treatment and without applied heat under UV radiation. 0.01Fe-TUD-1 performed 93.2% the highest conversion, but the conversion dropped as Fe increased. Ti-TUD-1 activity was much lower than Fe-TUD-1 since Fe is more active in the phenol hydroxylation under thermal treatment. 0.01Fe–0.01Ti-TUD-1 and 0.01Fe–0.03Ti-TUD-1 had high conversion up to 93.1 and 90.5%, respectively, giving HQ as the main product. The introduction of Fe into Ti-TUD-1 improved the ability of monometallic Ti-TUD-1 owing to high hydroxyl generator. Under UV radiation Fe species was not active enough to generate the extra hydroxyl radical,

hence 0.01Fe-TUD-1 showed only 14.3% conversion. The conversion of Ti-TUD-1 increased with increasing Ti content, exhibiting higher activity than thermal treatment due to light sensitive with electron/hole generation properties. Fe did not improve Ti-TUD-1 activity in bimetallic Fe–Ti-TUD-1 due to the lower activity of Fe species under mild conditions. BQ was found as a main product and no HQ was observed under UV light since BQ needs high energy to convert into HQ. Of all catalysts, 0.01Fe–0.01Ti-TUD-1 and 0.01Fe-TUD-1 performed the catalytic activity on phenol hydroxylation under thermal condition while Ti-TUD-1 improved activity under UV radiation. The leaching of metal ions in 0.01Fe–0.01Ti-TUD-1 sample according to metal extraframework and the presence of strong oxidant led to non-reusability and lack of hydrothermal stability.

## 6.6 Acknowledgements

This research is financially supported by the Thailand Research Fund through the Royal Golden Jubilee Scholarship (Grant No. PHD/0013/2554), the Ratchadapisake Sompote Endowment Fund, and the Center of Excellence for Petrochemical and Materials Technology, Chulalongkorn University, Thailand. The authors are also thankful to Mr. John M. Jackson and Mr. Benjamin A. De Armond for English proof-reading.

## 6.7 References

[1] Z. Shan, J.C. Jansen, W. Zhou, Th. Maschmeyer, Appl. Catal., A 254 (2003) 339-343.

[2] C. Aquino, Th. Maschmeyer, A New Family of Mesoporous Oxides-Synthesis, Characterisation and Applications of TUD-1. in: V. Valtchev, S. Mintova, M. Tsapatsis (Eds.), Ordered porous solids recent advances and prospects, Great Britain: Elsevier B. V., 2009, pp. 3-30.

[3] M. Balakrishnan, E. R. Sacia and A.T. Bell, Green Chem. 14 (2012) 1626–1634.

[4] I. Fechete, E. Gautron, E. Dumitriu, D. Lutic, P. Caullet, H. Kessler, Rev. Roum. Chim. 53 (2008) 49-54.

[5] R. Anand, M.S. Hamdy, U. Hanefeld, Th. Maschmeyer,Catal. Lett. 95 (2004) 113-117.

[6] X. Wang, C. Song, A.M. Gaffney, R. Song, Catal. Today 238 (2014) 95-102.

[7] M.S. Hamdy, G. Mul, J.C. Jansen, A. Ebaid, Z. Shan, A.R. Overweg, Th. Maschmeyer, Catal. Today 100 (2005) 255-260.

[8] M.S. Hamdy, G. Mul, W. Wei, R. Anand, U. Hanefeld, J.C. Jansen, J.A. Moulijn, Catal. Today 110 (2005) 264-271.

[9] R. Maheswari, M.P. Pachamuthu, R. Anand, J. Porous Mater. 19 (2012) 103-110.

[10] Z.X. Zhang, P. Bai, B. Xu, Z.F. Yan, J. Porous Mater.13 (2006) 245-250.

[11] Z. Shan, J.C. Jansen, L. Marchese, Microporous Mesoporous Mater. 48 (2001) 181-187.

[12] S. Telalović, A.Ramanathan, J.F. Ng, R. Maheswari, C. Kwakernaak, F. Soulimani, H.C. Brouwer, G.K. Chuah, B.M. Weckhuysen, U. Hanefeld, Chem. Eur. J. 17 (2011) 2077-2088.

[13] Y. Jiang, K. Lin, Y. Zhang, J. Liu, G. Li, J. Sun, X. Xu, Appl. Catal., A 445-446 (2012) 172-179.

[14] Á. Szegedi, Z. Kónya, D. Méhn, E. Solymár, G. Pál-Borbély, Z.E. Horváth, L.P. Biró, I. Kiricsi, Appl. Catal., A 272 (2004) 257-266.

[15] A. Wingen, N. Anastasievič, A. Hollnagel, D. Werner, F.J. Schüth, Catal. 193 (2000) 248-254.

[16] H. Liu, G. Lu, Y. Guo. Y. Guo, J. Wang, Nanotechnology 17 (2006) 997-1003.

[17] S. Shen, Y. Deng, G. Zhu, D. Mao, Y. Wang, G. Wu, J. Li, X. Liu, G. Lu, D. Zhao, J. Mater. Sci. 42 (2007) 7057-7061.

[18] G.D. Mihai, V. Meynen, E. Beyers, M. Mertens, N. Bilba, P. Cool, E. F. Vansant, J. Porous Mater. 16 (2009) 109-118.

[19] C.H. Rhee, J.S. Lee, Catal. Lett. 40 (1996) 261-264.

[20] W. Tanglumlert, S.T. Yang, K.E. Jeong, S.Y. Jeong, W.S. Ahn, Res. Chem. Intermed. 37 (2011) 1267-1273.

[21] F. Adam, J. Andas, I. Ab. Rahman, Chem. Eng. J. 165 (2010) 658-667.

[22] L.M. Mahoney, Photocatalysis studies using mesoporous modified V-MCM-48 Stober synthesis, PhD thesis, Kansas State University, 2010.

[23] M. Thommes, Chem. Ing. Tech. 82 (2010) 1059-1073.

[24] M.S. Hamdy. Functionalized TUD-1: Synthesis, characterization and (photo-) catalytic performance. in: J.A Moulijin, Th. Maschmeyer (Eds.), Synthesis and characterization of M-TUD-1 (M=Ti, V, Cr, Mo, Fe, Co and Cu) Easy formation of isolated catalytic sites and/or nano-particles embedded in mesoporous TUD-1, The Netherlands, 2005, pp. 27-72.

[25] A. Ramanathan , M.C.C. Villalobos, C. Kwakernaak, S. Telalovic, U. Hanefeld, Chem. Eur. J. 14 (2008) 961-972.

[26] A.Gervasini, C. Messi, P. Carniti, A. Ponti, N. Ravasio, F. Zaccheria, J. Catal. 262 (2009) 224-234.

[27] Y. Shao, L. Wang, J. Zhang, M. Anpo, J. Phys.Chem. B 109 (2005) 20835–20841.

[28] S. Haddoum, I. Fechete, B. Donnio, F. Garin, D. Lutic, C.E. Chitour,Catal. Commun. 27 (2012) 141-147.

[29] S. Haddoum, I. Fechete, B. Donnio, F. Garin, D. Lutic, C.E. Chitour, Catal. Commun. 27 (2012) 141-147.

[30] J. Zhou, Z. Hua, X. Cui, Z. Ye, F. Cui, J. Shi, Chem. Commun. 46 (2010) 4994-4996.

[31] S. Kulawong, S. Prayoonpokarach, A. Neramittagapong, J. Wittayakun, J. Ind. Eng. Chem. 17 (2011) 346-351.

[32] R. Klaewkla, S. Kulprathipanja, P.Rangsunvigit, T. Rirksomboon, W. Rathbun, L. Nemeth, Chem. Eng. J. 129 (2007) 21-30.

[33] P. Vollhardt, N. Schore, Organic Chemistry Structure and Function, sixth ed., W. H. Freeman and Company, New York, 2011.

[34] Y. Jia, W. Han, G. Xiong, W. Yang, Sci. Tech. Adv. Mater. 8 (2007) 106-109.

[35] S. Huixian, Z. Tianyong, L. Bin, W. Xiao, H. Meng, Q. Mingyan, Catal. Commun. 12 (2011) 1022-1026.

[36] H. El-Hamshary, M. H. El-Newehy, S. S. Al-Deyab, Molecules, 16 (2011) 9900-9911.

[37] C. Wu, Y. Kong, F. Gao, Y. Wu, Y. Lu, J. Wang, L. Dong, MicroporousMesoporous Mater. 113 (2008) 163-170.

[38] A. Wróblewska, Reac. Kinet. Mech. Cat. 108 (2013) 491-505.

[39] X. Ye, Y. Cui, X. Qiu, X. Wang, Appl. Catal., B 152-153 (2014) 383-389.

[40] C. Chiou, C. Wu, R. Juang, Chem. Eng. J. 139 (2008) 322-329.

[41] C. Adán, A. Bahamonde, I. Oller, S. Malato, A. Martínez-Arias, Appl. Catal., *B 144 (2014) 269-276.*

[42] R. Klaewkla, T. Rirksomboon, S. Kulprathipaja, L. Nemeth, P. Rangsunvigit, Catal. Commun.7 (2006) 260-263.

[43] K.M. Valkaj, O. Wittine, K. Margeta, T. Granato, A. Katović, S. Zrnčević, Pol. J. Chem. Technol. 3 (2011) 28-36.

[44] Y. Jiang, K. Jin, Y. Zhang, J. Liu, G. Li, J. Sun, X. Xu, Appl. Catal., A. 445-446 (2012) 172-179.

[45] M.P. Pachamuthu, V.V. Srinivasan, R. Maheswari, K. Shanthi, A. Ramanathan, Catal. Sci. Technol. 3 (2013) 3335.

[46] N. Serpone, J. phys. Chem B 110 (2006) 24287-24293.

[47] R. Oleksak, W.F. Stickle, G. Herman, J. Mater. Chem. C (2015) Accepted Manuscript, DOI: 10.1039/C4TC02985B.

[48] S. Artkla, W. Choi, J. Wittayakun, EnvironmentAsia 1 (2009) 41-48.